REVIEW

doi:10.1038/nature14453

The crystallography of correlated disorder

David A. Keen[1] & Andrew L. Goodwin[2]

Classical crystallography can determine structures as complicated as multi-component ribosomal assemblies with atomic resolution, but is inadequate for disordered systems—even those as simple as water ice—that occupy the complex middle ground between liquid-like randomness and crystalline periodic order. Correlated disorder nevertheless has clear crystallographic signatures that map to the type of disorder, irrespective of the underlying physical or chemical interactions and material involved. This mapping hints at a common language for disordered states that will help us to understand, control and exploit the disorder responsible for many interesting physical properties.

It is remarkable that, for all its indisputable successes, the language of classical crystallography still cannot properly describe the structure of water ice[1]. This inadequacy is clearly not a consequence of an especially complicated molecular structure or an enormous unit cell. Nor is it because water cannot be crystallized: snowflakes are as commonly recognized to be crystals as are rock salt and gemstones. Rather, it is because this chemically simple system challenges the very axiom on which classical crystallography rests: namely, the existence of translational periodicity. Though far from random, the orientations of water molecules in ice are not periodic. There is no space group to describe the local correlations that do persist; the very language of classical crystallography fails. Even the higher-dimensional abstractions that describe quasicrystals and incommensurate phases cannot help. Yet the relative orientations of neighbouring water molecules still shape the physical properties of ice because they govern its hydrogen-bonding network, its distribution of electric dipoles, and its anomalous configurational entropy—all of which would differ fundamentally were its structure entirely periodic.

Ice is by no means the only exception to the crystallographic rulebook, and many before us have already commented on the inadequacy of classical crystallography to describe important families of materials[2,3]. Indeed, one of our aims here is to highlight not only the progress that has been made in probing and understanding correlated disorder, but also the diversity of scientific domains in which it is assuming increasing importance. This diversity is reflected even in the dense packings of simple polyhedra, among which correlated disordered states now appear to be more common than crystalline phases[4]. Yet we are somewhat biased against the study of disordered states because our analytical techniques are so predisposed to order. In this sense the timing of our review is by no means accidental: the convergence of modern developments in crystallographic methods—experimental, computational and algorithmic—now provides the necessary insight into correlated disorder, so that long-standing problems in the field can at last be addressed. Moreover, just as classical crystallographic techniques can be applied across the sciences—to proteins and minerals and magnets alike—and the data understood and interpreted within one theoretical framework, so too do the diffraction patterns of materials with different types of correlated disorder hint at a common descriptive language for these states.

What emerges is that correlated disorder seems to arise in one of two scenarios. There may be an incompatibility between the interactions that drive order and the geometry of the lattice on which that order must evolve; this is the 'geometric frustration' well known in the field of frustrated magnetism. Alternatively, the dominant interactions in a system might be satisfied in sufficiently many ways that they do not encode a unique ordering pattern, as illustrated by the square ice model of Box 1 Figure. These two ordering problems—one of frustrated overconstraint and the other of configurational underconstraint—are related in that they both give rise to a degenerate manifold of ground states. This degeneracy results in a set of characteristic physical properties that emerge irrespective of the physical origin of the particular interactions involved: extreme susceptibilities, low-energy excitations, liquid-like behaviour and collective or emergent states. A second consequence is the distinction between local and average symmetry that is so often implicated in the unusual physical properties of disordered crystals (see also Box 1).

We begin our Review by explaining the experimental signature of correlated disorder (that is, diffuse scattering) and how it is measured and interpreted. Drawing on a wide range of examples, we establish qualitative mappings of problems of correlated disorder across ostensibly disparate fields. We show that such mappings concern not only the microscopic nature of correlated disorder but also the form of the diffraction patterns observed in crystallographic experiments. In this way, many of the crystallographic tools conventionally used to study periodic order can help us with the arguably more difficult problem of understanding disorder. Before concluding with a discussion of the opportunities and challenges for researchers in the field, we highlight how that central mantra of structural science—namely, that structure determines function—applies as much to correlated disordered states of matter as it does to crystals.

Scattering from disordered crystals

Crystal structures are determined by interpreting diffraction patterns obtained by scattering X-rays, neutrons or electrons from crystalline samples. The diffraction pattern of an ideal crystal and even of a quasicrystal and of an incommensurately modulated crystal is a set of discrete sharp Bragg reflections, whereas for the most disordered condensed phases (liquids or glasses) the scattering consists of smoothly continuous broad rings with no Bragg peaks at all. Crystal systems with

[1]ISIS Facility, Rutherford Appleton Laboratory, Harwell Oxford, Didcot, Oxfordshire OX11 0QX, UK. [2]Department of Chemistry, University of Oxford, Inorganic Chemistry Laboratory, South Parks Road, Oxford OX1 3QR, UK.

BOX 1

Correlated disorder in square ice

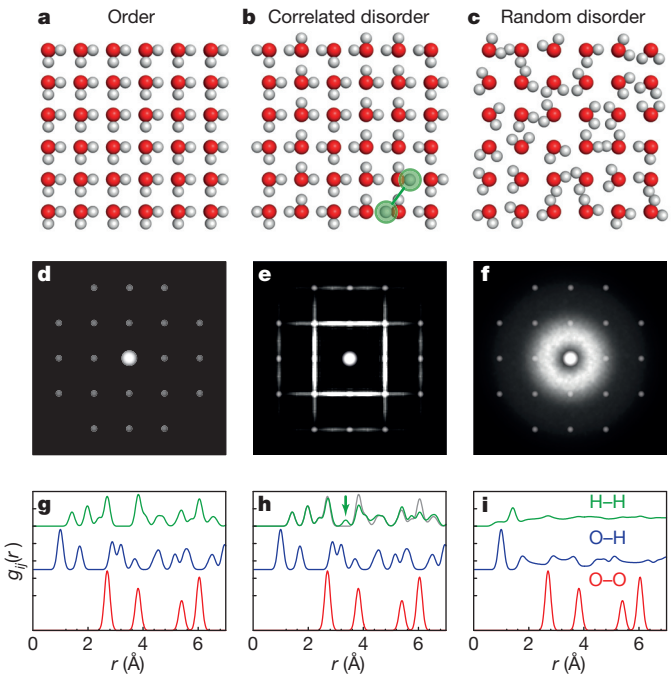

The figure shows how structures with correlated disorder (**b**, **e**, **h**) fall in between those with complete order (**a**, **d**, **g**) and those that are disordered randomly (**c**, **f**, **i**). The differences between the structures of the systems (**a**–**c**) are evident from the 'diffuse' scattering in their diffraction patterns (**d**–**f**) and from their PDFs (**g**–**i**). The example used is that of square ice, a simplified two-dimensional representation of the three-dimensional structure of water ice. Interestingly, this hypothetical square ice structure is similar to a phase very recently observed in thin layers of water trapped between graphene sheets[71]. Each oxygen atom (red) on a square grid is surrounded by four hydrogen atoms (white); two of these are covalently bonded and two are hydrogen-bonded to the oxygen atom. This simple rule, developed by Bernal and Fowler[72] and Pauling[40], might be expected to lead to an ordered structure (**a**). But the short-range nature of the rule means that structural variants as in **b**, with correlated disorder and residual low-temperature entropy[73], are more likely. The correlation in **b** involves all O–H bonds pointing along a common direction for each individual row and column; the structure is disordered because these directions are uncorrelated across rows or columns. The average crystallographic unit cell for square ice has two 50%-occupied hydrogen sites between each pair of oxygen sites. Since the repeating lattice is the same for structures **a**–**c**, their Bragg scattering, shown as grey dots in the X-ray diffraction plots in **d**–**f**, is essentially indistinguishable. It is therefore the broad or 'diffuse' scattering in plots **d**–**f**, and the pair distribution functions (plots **g**–**i**) that are sensitive to the differences between these structures. No diffuse scattering is observed for ordered structure **a** (plot **d**), whereas horizontal and vertical lines of diffuse scattering are produced by structure **b** from the locally correlated hydrogen atom positions (plot **e**). Structure **b** should be contrasted with a random arrangement of water molecule orientations on a square lattice (**c**), whose average unit cell would have a ring of hydrogen density around each oxygen site; this gives a broad ring of diffuse scattering centred at the origin (as in **f**), more akin to the familiar solvent ring seen in diffraction from proteins. Indeed, a diffuse ring like this would be the only feature in a diffraction pattern from two-dimensional 'liquid' water, because the lattice that gives rise to Bragg peaks would have melted. The equivalent partial PDFs are shown in **g**–**i** for **a**–**c**, respectively. These functions represent the probability of finding an atom of one type a certain distance away from an atom of another type and local deviations from the ideal lattice are clearly seen. For example, whereas all structures produce identical $g_{OO}(r)$ (red lines) reflecting the regular arrangement of oxygen atoms, subtle additional H–H peaks in **h** but not in **g** (green lines; the $g_{HH}(r)$ from **g** is reproduced in **h** as a thin grey line) are characteristic of specific correlations that exist in structure **b** but not in structure **a**. One such H–H correlation (green arrow in **h**) is highlighted in green in **b**. (The PDFs were calculated with a representative 'experimental' Gaussian broadening. Diffuse scattering was calculated using Discus[19].)

correlated disorder produce diffraction patterns that contain discrete Bragg reflections as well as continuous scattering. It is this structured continuous (or 'diffuse') scattering that reflects the correlations present in the disordered component, yet classical crystallography gives no recipe for its analysis. If, as is often the case, this component is simply ignored and conventional approaches are used to measure and interpret the Bragg peak intensities, then the structural model obtained represents a configurational average over all possible disordered states and any information concerning correlation is lost (see also discussion in Box 1).

Experimentally, diffuse scattering is collected using methods that survey large swathes of reciprocal space. In the early days, typified by the extensive investigations of Lonsdale[5,6], polychromatic ('Laue') or monochromatic X-ray beams, single crystals and photographic film were employed in long-exposure experiments to reveal the diffuse features that are typically two to four orders of magnitude weaker than Bragg reflections. Nowadays large-area detectors have replaced film, and X-ray synchrotron instrumentation can collect three-dimensional volumes of high-quality reciprocal-space data extremely rapidly[7,8]. Similar neutron and electron reciprocal-space survey data can be measured using instruments such as the SXD instrument at ISIS[9,10] and transmission electron microscopes[11], respectively.

A measurement from a crystalline powder or large collection of nanocrystals averages the scattering volume into a one-dimensional diffraction pattern. Such 'total scattering' measurements are the powder equivalent of the surveying methods described above and have become increasingly popular in the past 25 years. They yield absolutely normalized diffraction patterns that contain all Bragg and diffuse scattering—the 'total scattering structure factor'. The Fourier transform of this function is the pair distribution function (PDF): a weighted sum of partial pair distribution functions, each of which describes the probability of finding atoms of one type a certain distance away from atoms of another type[12,13]. This very intuitive function (see Box 1) is important for understanding disordered crystal structures since it is one of the few measurable functions that directly accesses the key distances that are longer than those between bonded atoms (which fall within the domain of extended X-ray absorption fine structure and nuclear magnetic resonance measurements) and shorter than those which begin to reflect longer-range periodicity (tractable through analysis of Bragg peak intensities alone). Moreover, measurement and interpretation of a PDF need not draw on the assumptions of complete periodic order inherent to classical crystallography.

A relatively large number of instruments specifically designed for total scattering measurements have been commissioned at neutron sources, X-ray synchrotrons and by commercial companies making diffractometers for laboratory use. This is due to an increased awareness of the scientific merits of a total scattering experiment by crystallographers who

are starting to tackle structural problems that involve correlated disorder and, as a result, have demanded better instrumentation and greater access. Neutron diffractometers at time-of-flight sources produce the highest quality PDFs because they reach the highest possible momentum transfers Q: with the real-space resolution Δr of the PDF proportional to $1/Q_{max}$ and using $Q_{max} \approx 50$ Å^{-1}, data reaching a real-space resolution of $\Delta r \approx 0.1$ Å are routinely measurable. Moreover, these data can be placed on an absolute scale, which allows direct comparison with PDFs determined from candidate structural models. PDF methods have now become part of the toolkit not only for neutron diffraction but also for mainstream crystallography, thanks to the high-energy X-rays available at X-ray synchrotrons that permit routine and rapid collection of high-quality X-ray total scattering data[14,15]. The latter are limited in comparison to neutron data by the lower accessible values of $Q_{max} \approx 35$ Å^{-1} and the much reduced signal at high Q that results from the X-ray form factors. However, as in classical crystallographic studies, it is now increasingly common for neutron and X-ray total scattering data to be analysed in tandem. This is beneficial because different weightings lead in many cases (such as metal organic frameworks[16]) to different atom pairs dominating the neutron and X-ray PDFs.

Improved resolution and accuracy, and availability of X-ray and neutron data all help in the interpretation of the 3–10 Å region of the PDF that plays a key part in correlated disordered systems. However, perhaps most important is the development of modelling methods to interpret total scattering patterns.

Methods of analysing diffuse scattering

Interpretation of the diffuse contribution to diffraction patterns of disordered materials has typically been carried out on a case by case basis: experimenters observe diffuse scattering features and develop tools, which are often sample specific, for analysing their measurements with varying degrees of sophistication. Established protocols typically only consider small local defects or modulated deviations from the average periodicity, so such analyses are highly intuitive as there are no generic analytical methods for characterizing correlated disordered states. This said, one approach that has come to prominence recently is the 'real-space Rietveld' method implemented within the PDFGui computer program[17] that allows refinement of average-structure-like parameters (such as the unit cell and atom coordinates) against the PDF. Though the resulting structure is based on a periodic unit cell (this is the 'small box' of small-box modelling), the parameters are influenced by the local correlations captured in the low-r part of the PDF.

Many methods are limited in that their parameterized structural disorder may or may not be compatible with a physical arrangement of atoms. Analyses that construct or refine a 'big-box' model—typically a large supercell of the underlying crystal unit cell—are better able to generate a holistic picture of complex disordered states. These methods have become tractable with increases in computer power and the development of effective strategies for calculating single-crystal diffuse scattering patterns[18,19]. Monte Carlo calculations can now be tested with[20,21], and interaction potential parameters refined against[22], experimental diffuse scattering data. Diffuse scattering patterns can also be calculated for configurations generated during molecular dynamics simulations and subsequently compared against experimental data, an approach used in studies of silver-ion conductors[23] and organic semiconductors[24]. Diffuse scattering calculated[25] from *ab initio* phonon energies and eigenvectors has also been compared to experimental data[26], and mean-field formulations have been used for magnetic diffuse scattering calculations[27].

The reverse Monte Carlo method[28,29] refines 'big-box' models against experimental data by minimizing, using Monte Carlo protocols, the difference between functions calculated from the box of atoms and those determined experimentally. The appeal of the method lies with its generality and flexibility: no symmetry is enforced apart from periodic boundary conditions and the overall shape of the model, and constraints or restraints are only built into the method as needed. Also, any function that might be calculated from an atomistic model can be incorporated into the calculation of the agreement function. This is especially useful for disordered materials because both the Bragg profile (long-range periodicity) and total scattering functions (short-range disorder) can readily be calculated and used. The resulting refined 'big-box' model represents a snapshot of the disordered crystal structure, containing local correlations consistent with the measured total scattering while also replicating the average structure as revealed by the Bragg profile. It is a snapshot of the structure because the interaction between the X-ray (or neutron) and the sample is very fast on the timescale of atomic vibrations and because the total scattering function is predicated on a measurement that integrates over all energy changes in the material. This means that all disordering processes (whether dynamic or static) are captured within the reverse Monte Carlo refined model.

Mapping of apparently unrelated problems

If the presence of correlated disorder gives rise to structured diffuse scattering and/or unexpected pair correlations in the PDF, then it makes sense to investigate the relationship in reverse. That is, to what extent might diffuse scattering patterns or variations in the PDF be diagnostic of specific forms of correlated disorder?

Frustrated overconstraint

Our attempt to answer this question begins by considering the particular type of disorder associated with geometric frustration, typified by the problem of the Ising triangular antiferromagnet. A triangular array of Ising 'spins' (which can assume one of only two possible states, 'up' and 'down') is frustrated if energy is minimized by neighbouring spins adopting opposite states: each pair of opposing neighbours also share a third common neighbour, which cannot oppose both spins in the pair at once (Fig. 1a). The energy minimum for this system corresponds to a compromise situation in which each spin opposes, on average, only four of its six nearest neighbours and is forced to point in the same direction as the other two (hence 'frustration'). Figure 1b sketches one representative solution, but there are so many equivalent states that the system is characterized by a finite residual entropy at 0 K (ref. 30).

Despite the absence of long-range order amongst this family of ground states, the spin arrangements in a triangular Ising antiferromagnet remain correlated and are not random. Indeed, correlations with certain periodicities are very much stronger than others, resulting in a diffraction pattern that contains stronger scattering at points in reciprocal space that reflect these favoured periodicities. In this case, the scattering is particularly structured because it traces the Brillouin zone boundary of the underlying triangular lattice, reflecting the basic alternation in Ising state from one lattice site to the next. The absence of Bragg reflections means that no structure solution is possible from this scattering pattern using conventional techniques and there is no 'unit cell' that can describe the spin arrangement. Instead, a direct Fourier transform of the scattering function gives what is perhaps the closest equivalent: a two-dimensional spin correlation function representing the 'average local structure' of the disordered state[31].

The Ising model can be equally meaningfully applied across a range of systems beyond the field of magnetism. A problem of vacancy ordering, for example, might be described by the distribution of occupied (Ising 'up') and vacant (Ising 'down') sites, with the corresponding 'antiferromagnetic' interaction involving strain-driven anti-clustering of vacancies. Likewise, the arrangement of cations of two different formal charges (for example, 2+ = 'up', 3+ = 'down') might be dictated by the stronger Coulombic repulsion of the more highly charged component. In both cases one anticipates the realization of complex states in which the vacancy or charge localization can be mapped onto the spin states of the triangular Ising antiferromagnet, with the corresponding diffraction patterns—if measured using a probe of relevant sensitivity—reflecting the same structured diffuse scattering pattern associated with that canonical system. In this way, the form of the diffuse scattering pattern becomes a characteristic signature of a particular type of correlated

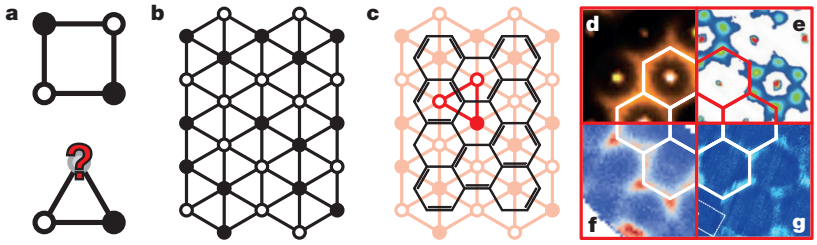

Figure 1 | Correlated disorder in the Ising triangular lattice. **a**, A lattice of sites in one of two states (such as spin up or spin down; here, black or white), adopts a complex structure wherever there is an incompatibility between the interaction of neighbours and the lattice geometry. 'Antiferromagnetic' interactions—favouring a reversal in state between neighbours—are easily satisfied on a square lattice (top) but cannot be fully satisfied on a triangular lattice (bottom). **b**, The compromise that emerges for an extended triangular lattice is for each triangle to adopt either a one-up-two-down or a one-down-two-up arrangement; one possible solution is shown here, though many others exist. **c**, There is a one-to-one mapping between these Ising states and the possible arrangements of π bonds in the resonating valence bond model for graphene: the π bonds are simply associated with the 'ferromagnetic' pairs on each triangle. **d**–**g**, Such mappings mean that qualitatively similar scattering functions are observed for structurally complex systems wherever that complexity has the same fundamental geometric origin. The packing arrangement of the Gag protein[8] (**d**), the orbital orientations in $Ba_3CuSb_2O_9$ (ref. 32) (**e**), the emergent spin structure of β-Mn (ref. 27) (**f**) and the electronic structure of graphene itself[33] (**g**) all map onto the problem of the Ising triangular antiferromagnet. Here, their X-ray (**d**, **e**), polarized neutron (**f**) and angle-resolved photoemission (**g**) scattering patterns all reveal the population of configurational, magnetic or electronic states with periodicities at the Brillouin zone boundary (solid white or red lines).

disorder that in itself might be taken to reflect a conceptual mapping among related problems of geometric frustration.

Such mappings are borne out in practice. In its crystal structure, the amino-terminal fragment of the Gag protein from Feline Foamy Virus packs on a triangular lattice with neighbouring fragments oriented in opposite directions in order to maximise packing efficiency[8]. Here the frustration involves fragment orientations, and the mapping onto the Ising problem is evident in the form of the structured diffuse scattering in X-ray diffraction patterns (Fig. 1d). In Co-doped β-Mn, ferromagnetically coupled multi-spin rods behave as collective magnetic entities that are themselves antiferromagnetically coupled. Because the multi-spin rods are arranged on a triangular lattice, the emergent spin structure is frustrated, with only the part of the spin-polarized single-crystal neutron scattering pattern sensitive to the magnetic structure containing diffuse scattering at the zone boundary (Fig. 1f)[27]. Geometric frustration of Jahn–Teller-distorted Cu^{2+} ions in $Ba_3CuSb_2O_9$ actually maps the problem of orbital order in this system onto the same Ising configurations, giving rise to a qualitatively similar scattering function (Fig. 1e)[32]. A final example involves the electronic band structure of graphene and its analogues: the well-established correspondence between the resonating valence bond model and the Ising triangular antiferromagnet (Fig. 1c) means that the momentum distribution of bonding states observed using angular-resolved photoemission spectroscopy also reveals the same distinctive pattern in reciprocal space (Fig. 1g)[33].

Despite the obvious similarity in the scattering patterns of these diverse systems, there remain important differences in the scattering detail. On the very simplest level, it is known that the positions of the scattering maxima reflect the nature and strength of next-nearest-neighbour correlations; likewise the widths of the features are sensitive to the concentration of Ising excitations[8]. It is in this sense that the structure refinement tools outlined in 'Methods of analysing diffuse scattering' can provide useful physical insight beyond the qualitative mappings of Fig. 1. Some of this sensitivity remains even for polycrystalline samples; the corresponding PDFs (or spin correlation functions for magnetic systems) are sensitive to longer-range interactions and may provide a direct measurement of correlation length[34].

Geometric frustration can and does emerge in many different systems with varying types of degrees of freedom and interactions well beyond those of the Ising triangular antiferromagnet. Historically, much of the emphasis has been on frustrated magnetism, because even within this individual field there are so many types of spin system (such as Ising, *XY*, Potts and Heisenberg), spin interaction (such as ferromagnetic, antiferromagnetic and bilinear–biquadratic), and lattice geometries (such as triangular, kagome, hyperkagome, pyrochlore) that the variety of complex magnetic states accessible in theory is large indeed[35]. Yet the part played by geometric frustration in governing a range of other types of ordering phenomena is becoming increasingly clear: examples include orbital order in the colossal magnetoresistance manganites[36], orientational correlations in plastic crystals[37], and collective transport properties of superionics[38] and elements alike[39]. As for the Ising triangular antiferromagnet, what emerges is that the underlying lattice geometry influences both the particular type of configurational degeneracy and also the basic form of the diffuse scattering observed experimentally.

Configurational underconstraint

This duality of conceptual and empirical mappings is often illustrated using materials based on the pyrochlore lattice of connected tetrahedra. In many ways cubic ice can be considered the parent of this family of materials: the relationship between its structure and that of the pyrochlore lattice can be seen by considering the network formed by the midpoints between connected oxygen atoms (Fig. 2a). The need for water molecules to be arranged so that each oxygen atom is connected to four hydrogen atoms, two of them covalently bonded and the other two hydrogen-bonded, results[40] in a disordered arrangement of H_2O molecule orientations, with each arrangement uniquely characterized by the choice of one particular edge per pyrochlore tetrahedron (shown in bold in Fig. 2a). It is a direct consequence of the ice rules that none of these edges meet; there is a one-to-one correspondence between unconnected edge decorations of the pyrochlore lattice and cubic ice configurations. In a similar way, both the direction of Cd^{2+} ion displacements in cubic $Cd(CN)_2$ and the arrangement of Ho^{3+} spins in $Ho_2Ti_2O_7$ can be mapped onto these same edge decorations (Fig. 2b and c). These three systems then share the same type of configurational degeneracy, and the terms 'charge ice' and 'spin ice' are used to describe the families of materials of which $Cd(CN)_2$ (ref. 41) and $Ho_2Ti_2O_7$ (ref. 42) are examples. Once again, these mappings amongst equivalent disordered states are reflected in the experimental diffuse scattering patterns. Water, charge, and spin ices all give rise to the same characteristic type of scattering pattern (Fig. 2e–g), with higher-order correlations and particulars of the scattering physics affecting the distribution of scattering intensity throughout reciprocal space[43]. That a qualitatively similar scattering pattern is associated with some superionic conductors (Fig. 2d) suggests that local correlations also have a role in these materials, even if the specific mechanism involved remains controversial[44].

Symmetry mismatch and local disorder

What is common to all these systems is that there exists a distinction between local symmetry and the (higher) average symmetry imposed by the crystal lattice. Individual water molecules have lower point symmetry than the tetrahedral crystallographic sites on which they sit in solid ice; likewise, the two-up-one-down compromise of the Ising antiferromagnet

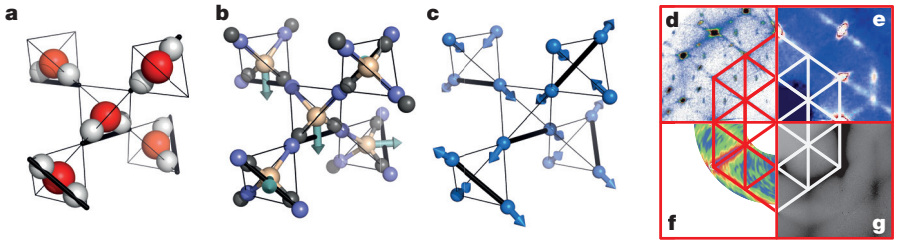

Figure 2 | Ice-like states on the pyrochlore lattice. **a**, The structure of cubic ice is related to that of the pyrochlore lattice (thin black lines). Many different orientations of the water molecules are capable of satisfying the same hydrogen-bonding 'rules', in which each configuration can be represented uniquely by decorating the edges associated with the two hydrogen atoms per tetrahedron (thick black lines). The ice rules are encoded in the provision that no two such edges join. **b**, **c**, The arrangement of dipoles in 'charge-ices' (**b**) and magnetic moments in 'spin-ices' (**c**) map onto the same edge decorations, linking the structural complexity of these physically disparate systems. **d**–**g**, Diffraction patterns of the superionic conductor α-$Cu_{1.8}Se$ (ref. 67) (**d**), the negative thermal expansion 'charge-ice' $Cd(CN)_2$ (ref. 41) (**e**), the quantum spin ice candidate $Yb_2Ti_2O_7$[68] (**f**) and (water) ice itself[69] (**g**) all show continuous scattering in related regions of reciprocal space.

breaks the threefold symmetry of the triangular lattice. The impact of this symmetry mismatch is for the average structure—deduced from analysis of Bragg diffraction—to appear to have a higher symmetry than that observed using local spectroscopic probes or expected from crystal chemical considerations. This has led to misconceptions about disordered crystal structures in the past (for example, the apparently linear Si–O–Si bond in β-cristobalite[45]), and the clearest way to address this ambiguity is through direct analysis of the diffuse scattering or through modelling of the total scattering. Big-box modelling is particularly effective because local distortions within individual unit cells can be explored (to agree with PDF data, for example) while still generating an overall structure that replicates the Bragg diffraction intensities.

Such an approach has been used to address high-temperature behaviour in ferroelectric $BaTiO_3$: even within the cubic (paraelectric) phase the Ti atoms are displaced from the centre of the TiO_6 octahedron in one of the eight ⟨111⟩ directions, mimicking the distorted arrangement of the ordered low-temperature rhombohedral phase[46]. These eight Ti positions average to the central octahedral B-site in the ideal perovskite structure (Fig. 3a)[47]. A similar conclusion was reached in studies of the thermoelectric properties of PbTe (which has the same structure as rock salt) in terms of large-amplitude displacements of Pb atoms along ⟨100⟩-type directions at high temperature[48]. Likewise, the high ionic conductivity of δ-Bi_2O_3 was shown to depend on local relaxation of the Bi-ion coordination geometry towards that adopted in the low-temperature β-phase; these correlated distortions promote vacancy migration (Fig. 3b)[49]. The Bi atoms in the relaxor ferroelectric NBT ($Na_{0.5}Bi_{0.5}TiO_3$) also assume positions of lower local symmetry than that of the average lattice in the rhombohedral phase[50]. These are all examples where second-order Jahn–Teller distortions of the Bi^{3+}, Pb^{2+} and Ti^{4+} coordination environments are responsible for lowering the local symmetry. Analogous behaviour is observed for molecular systems where a phase transition can only reduce the overall structural distortion and raise the average symmetry through a superposition of distinct molecular orientations. An example of this is seen in Fig. 3c where rotational disorder in the imidazolium cation $(C_3H_5N_2)^+$ above the ferroelectric phase transition leads to an average hexagonal molecular shape that is chemically nonsensical[51].

For most materials correlated disorder persists only in a high-temperature state, with order emerging on cooling. But in some systems the disordered state is trapped to low temperatures. One example is $K_{1-x}(NH_4)_xI$ (with $x \approx 0.5$), where the tetrahedral geometry of the ammonium cation is incompatible with the octahedral symmetry of its crystallographic site in the rock salt structure[52]. A second example is solid C_{60}, where the combination of icosahedral molecular symmetry and trigonal point symmetry at the crystallographic site frustrates order and gives rise to glassy dynamics at low temperatures[53]. A similar mismatch between symmetry at the molecular and crystal lattice level also exists in far larger structures, and is even exploited in the mechanical release of phage DNA from viruses[54].

Disorder–property relationships

Perhaps counterintuitively, correlated disorder may actually be an essential ingredient for functional material properties. There will be even more cases where disorder—though not by itself the microscopic driving force—is intimately associated with a particular functionality. Any switchable ferroic state, for example, emerges from a disordered parent phase where the correlations that are present describe the ferroic property of interest. Relaxor ferroelectrics are an extreme example of this relationship, where correlations are so strong that they stabilize polar nanoregions, which in turn drive the attractive dielectric properties for which relaxors are favoured[55]. Here it is dipolar disorder that results in function, but there are strong analogies too to the balance of orbital, electronic, and magnetic disorder implicated in the colossal magnetoresistance of $La_xCa_{1-x}MnO_3$, for example[56]. Likewise, the proximity of correlated paramagnetic states to the superconducting transitions of most high-temperature superconductors has been noted many times previously (for example, see ref. 57). As these examples illustrate, there is at least an empirical correspondence between correlated disorder and advanced function that is increasingly obvious even if not yet well understood.

Correlated disorder is often implicated in cooperative phenomena. One example is solid-phase ion conduction: superionics are effectively porous to a particular type of ion precisely because there exists a low-barrier mechanism for collective displacements. Another example is the emergence of quasi-particles such as skyrmions in chiral ferromagnets[58] and magnetic 'monopoles' in the pyrochlore spin ices[59], and the potential application of these phenomena in data storage and spintronic devices would constitute putting correlated disorder to practical use. As a final point, we note that the configurational entropy associated with disordered states has its own set of thermodynamic and lattice dynamical consequences that affect material properties. Not only would ice melt at a different temperature were it not for proton disorder, but the influence of disorder on phonons is exploited in optimizing thermal conductivity of thermoelectrics[60].

Concluding remarks

As we have shown here, simple local rules or distortions can give rise to surprisingly complex disordered states of matter in a wide range of material systems. In many cases the presence of disorder—whether chemical, electronic, magnetic or geometric—and the nature of the correlations that persist within the disordered phase affect the physical and chemical properties of the system in question. Just as classical crystallography has helped us to develop an understanding of the structures of ordered crystalline materials, so modern crystallography and its ever-improving methods are rapidly improving our ability to characterize

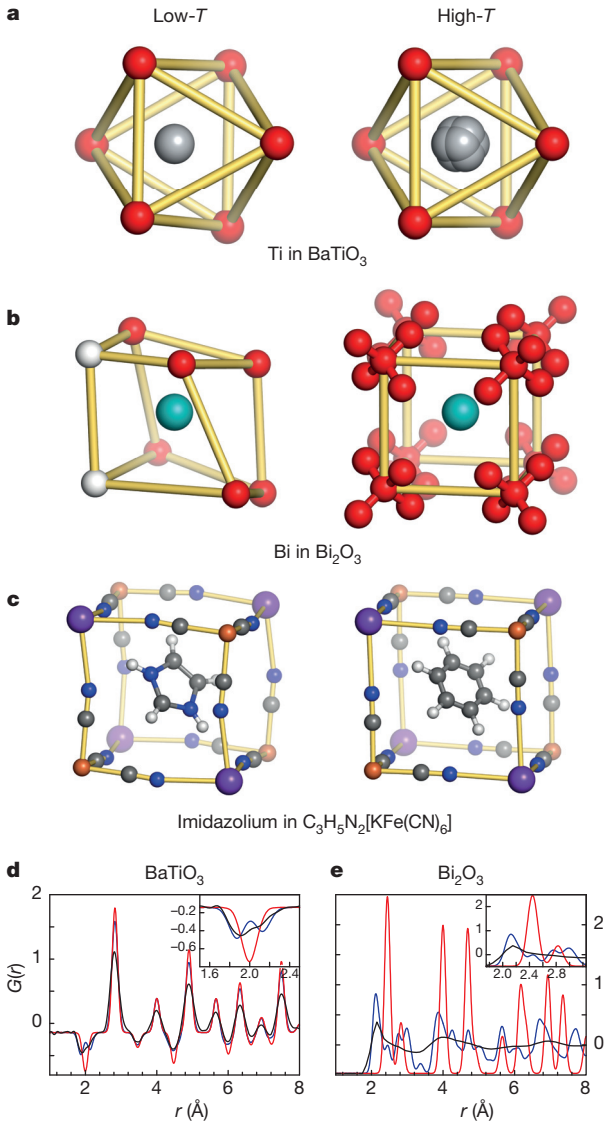

Figure 3 | Local symmetry mismatch. **a**–**c**, Examples of phase transitions where mismatch is resolved at low temperature T through lowering of the lattice symmetry and high-temperature average structures rely on descriptions involving partially occupied sites (see main text for details). **a**, Ti in $BaTiO_3$; **b**, Bi in Bi_2O_3; and **c**, imidazolium in $(C_3H_5N_2)_2[KFe(CN)_6]$. The experimental pair distribution functions $G(r)$ (black lines) from **a** and **b** at high temperature are compared with the $G(r)$ values calculated using PDFGui[17] from the average structures of the phases at low (blue lines) and high (red lines) temperatures in **d** and **e**, respectively. In each case the low-r portion of the measured high-temperature phase $G(r)$ more closely resembles that calculated from the average structure of the low-temperature phase (see insets to **d** and **e**). Reference structures are: **a**, average structures[70] for the low-temperature $R3m$ phase and the high-temperature cubic $Pm\bar{3}m$ phase; **b**, average structures at 297 K ($P\bar{4}2_1c$, β-phase) and 1,033 K ($Fm\bar{3}m$, δ-phase)[49]; **c**, for the order–disorder transition from $(C_3H_5N_2)_2[KFe(CN)_6]$ at 83 K ($C2/c$) and 293 K ($R\bar{3}m$)[51]; **d**, PDF data (J. A. Hriljac and D.A.K., unpublished work); and **e**, PDF data[49].

and interpret correlated disorder. We take encouragement from the observation that certain types of correlated disorder recur in completely different fields. This recurrence of specific forms of disorder hints at the possibility of a universal language for describing correlated disordered states, much like the space groups of classical crystallography.

Beyond even the problem of correlated disorder lie exotic states of matter with varying degrees of order and disorder over vastly different (and often multiple) length scales. Meeting the challenge of structurally characterizing such phases will require further development of the 'small angle' scattering techniques that probe larger-scale structures. Ever larger structural models will be needed to aid the interpretation of data from instruments such as NIMROD at ISIS[61] that can measure total scattering to much smaller values of Q. Furthermore, as correlated disorder is investigated in ever more complicated systems, there will be an increasing demand for analysis based on effective interfacing of different techniques: the combined analysis of extended X-ray absorption fine structure, total scattering and single-crystal diffuse scattering will reveal more than each type of data could reveal individually. This convergence of different methods of analysis is beginning to happen[62], and comparative PDF and single-crystal diffuse scattering studies of molecular systems[63,64] have highlighted the value of programs[19,29] able to incorporate both data types[65]. The possibility of extracting the three-dimensional PDF from single-crystal measurements is a particularly exciting development in the field[66], because it removes the limitation of orientational averaging inherent to all powder methods.

Ultimately, of course, the goal will be to control and exploit correlated disorder. This reverses the paradigm of seeking to understand the disorder responsible for interesting physical properties to one of intentionally employing it as a design element in its own right, in order to engineer materials with novel functionalities. But the crucial first step towards that goal is developing the ability to fully characterize correlated disorder, and we hope that our review has shown how such studies might be initiated and will encourage others to join in with this important branch of modern crystallography.

Received 31 July 2014; accepted 13 March 2015.

1. Kuhs, W. F. & Lehmann, M. S. The structure of ice-Ih. *Water Sci. Rev.* **2,** 1–66 (1986).
2. Cartwright, J. H. E. & Mackay, A. L. Beyond crystals: the dialectic of materials and information. *Phil. Trans. R. Soc. Lond. A* **370,** 2807–2822 (2012).
3. Bernal, J. D. & Carlisle, C. H. The range of generalised crystallography. *Sov. Phys. Crystallogr.* **13,** 811–831 (1969).
4. Damasceno, P. F., Engel, M. & Glotzer, S. C. Predictive self-assembly of polyhedra into complex structures. *Science* **337,** 453–457 (2012).
5. Lonsdale, K. & Smith, H. An experimental study of diffuse X-ray reflexion by single crystals. *Proc. R. Soc. A* **179,** 8–50 (1941).
6. Lonsdale, K. X-ray study of crystal dynamics: an historical and critical survey of experiment and theory. *Proc. Phys. Soc.* **54,** 314–353 (1942).
7. Maisel, S. B., Schindzielorz, N., Müller, S., Reichert, H. & Bosak, A. An accidental visualization of the Brillouin zone in an Ni-W alloy via diffuse scattering. *J. Appl. Cryst.* **46,** 1211–1215 (2013).
8. Welberry, T. R., Heerdegen, A. P., Goldstone, D. C. & Taylor, I. A. Diffuse scattering resulting from macromolecular frustration. *Acta Crystallogr. B* **67,** 516–524 (2011).
   This elegantly describes how a complicated diffuse scattering pattern might be explained in terms of simple disordering rules.
9. Welberry, T. R. *et al.* Diffuse neutron scattering in benzil, $C_{14}D_{10}O_2$, using the time-of-flight Laue technique. *J. Appl. Cryst.* **36,** 1440–1447 (2003).
10. Keen, D. A., Gutmann, M. J. & Wilson, C. C. SXD—the single crystal diffractometer at the ISIS Spallation Neutron Source. *J. Appl. Cryst.* **39,** 714–722 (2006).
11. Withers, R. L. Disorder, structured diffuse scattering and the transmission electron microscope. *Z. Kristallogr.* **220,** 1027–1034 (2005).
12. Soper, A. K. & Barney, E. R. Extracting the pair distribution function (PDF) from white beam X-ray total scattering data. *J. Appl. Cryst.* **44,** 714–726 (2011).
13. Keen, D. A. A comparison of various commonly used correlation functions for describing total scattering. *J. Appl. Cryst.* **34,** 172–177 (2001).
14. Chupas, P. J. *et al.* Rapid-acquisition pair distribution function (RA-PDF) analysis. *J. Appl. Cryst.* **36,** 1342–1347 (2003).
15. Skinner, L. B., Benmore, C. J. & Parise, J. B. Area detector corrections for high quality synchrotron X-ray structure factor measurements *Nucl. Instrum. Meth. A* **662,** 61–70 (2012).
16. Bennett, T. D. *et al.* Structure and properties of an amorphous metal-organic framework. *Phys. Rev. Lett.* **104,** 115503 (2010).
17. Farrow, C. L. *et al.* PDFfit2 and PDFgui: computer programs for studying nanostructure in crystals. *J. Phys. Condens. Matter* **19,** 335219 (2007).
18. Butler, B. D. & Welberry, T. R. Calculation of diffuse scattering from simulated disordered crystals: a comparison with optical transforms. *J. Appl. Cryst.* **25,** 391–399 (1992).
19. Neder, R. B. & Proffen, T. *Diffuse Scattering and Defect Structure Simulations: A Cook Book using the Program DISCUS* (Oxford Univ. Press, 2008).
20. Goossens, D. J., Heerdegen, A. P., Chan, E. J. & Welberry, T. R. Monte Carlo modeling of diffuse scattering from single crystals: the program ZMC. *Metall. Mater. Trans. A* **42,** 23–31 (2011).
21. Welberry, T. R., Chan, E. J., Goossens, D. J. & Heerdegen, A. P. Use of Monte Carlo simulation for the interpretation and analysis of diffuse scattering. *Phase Transit.* **83,** 80–98 (2010).

22. Chan, E. J. *et al.* Single-crystal diffuse scattering studies on polymorphs of molecular crystals. I. The room-temperature polymorphs of the drug benzocaine. *Acta Crystallogr. B* **65,** 382–392 (2009).
23. Welberry, T. R. & Paściak, M. Monte Carlo and molecular dynamics simulation of disorder in the Ag^+ fast ion conductors pearceite and polybasite. *Metall. Mater. Trans. A* **42,** 6–13 (2011).
24. Eggeman, A. S., Illig, S., Troisi, A., Sirringhaus, H. & Midgley, P. A. Measurement of molecular motion in organic semiconductors by thermal diffuse electron scattering. *Nature Mater.* **12,** 1045–1049 (2013).
25. Xu, R. & Chiang, T. C. Determination of phonon dispersion relations by X-ray thermal diffuse scattering. *Z. Kristallogr.* **220,** 1009–1016 (2005).
26. Gutmann, M. J. *et al.* Room temperature single-crystal diffuse scattering and ab initio lattice dynamics in $CaTiSiO_5$. *J. Phys. Condens. Matter* **25,** 315402 (2013).
27. Paddison, J. A. M. *et al.* Emergent frustration in Co-doped β-Mn. *Phys. Rev. Lett.* **110,** 267207 (2013).
Reverse Monte Carlo analysis of an experiment uncovers an unexpected magnetic structure with a simple underlying basis.
28. McGreevy, R. L. Reverse Monte Carlo modelling. *J. Phys. Condens. Matter* **13,** R877–R913 (2001).
29. Tucker, M. G., Keen, D. A., Dove, M. T., Goodwin, A. L. & Hui, Q. RMCProfile: reverse Monte Carlo for polycrystalline materials. *J. Phys. Condens. Matter* **19,** 335218 (2007).
30. Wannier, G. H. Antiferromagnetism. The triangular Ising net. *Phys. Rev.* **79,** 357–364 (1950).
31. Paddison, J. A. M., Stewart, J. R. & Goodwin, A. L. SPINVERT: a program for refinement of paramagnetic diffuse scattering data. *J. Phys. Condens. Matter* **25,** 454220 (2013).
32. Nakatsuji, S. *et al.* Spin-orbital short-range order on a honeycomb-based lattice. *Science* **336,** 559–563 (2012).
33. Rasche, B. *et al.* Stacked topological insulator built from bismuth-based graphene sheet analogues. *Nature Mater.* **12,** 422–425 (2013).
34. Paddison, J. A. M. *et al.* Spin correlations in $Ca_3Co_2O_6$: polarized-neutron diffraction and Monte Carlo study. *Phys. Rev. B* **90,** 014411 (2014).
35. Lacroix, C., Mendels, P. & Mila, F. *Introduction to Frustrated Magnetism: Materials, Experiments, Theory* (Springer, 2011).
36. Lynn, J. W. *et al.* Order and dynamics of intrinsic nanoscale inhomogeneities in manganites. *Phys. Rev. B* **76,** 014437 (2007).
37. Shintani, H. & Tanaka, H. Frustration on the way to crystallization in glass. *Nature Phys.* **2,** 200–206 (2006).
38. Wood, B. C. & Marzari, N. Dynamical structure and thermodynamics of the superionic sublattice in α-AgI. *Phys. Rev. Lett.* **97,** 166401 (2006).
39. Ogitsu, T., Schwegler, E. & Galli, G. β-rhombohedral boron: at the crossroads of the chemistry of boron and the physics of frustration. *Chem. Rev.* **113,** 3425–3449 (2013).
40. Pauling, L. The structure and entropy of ice and of other crystals with some randomness of atomic arrangement. *J. Am. Chem. Soc.* **57,** 2680–2684 (1935).
41. Fairbank, V. E., Thompson, A. L., Cooper, R. I. & Goodwin, A. L. Charge-ice dynamics in the negative thermal expansion material $Cd(CN)_2$. *Phys. Rev. B* **86,** 104113 (2012).
42. Bramwell, S. T. *et al.* Spin correlations in $Ho_2Ti_2O_7$: a dipolar spin ice system. *Phys. Rev. Lett.* **87,** 047205 (2001).
One of the first experimental papers that initiated the studies of spin ices and subsequent searches for magnetic monopoles.
43. Fennell, T. *et al.* Magnetoelastic excitations in the pyrochlore spin liquid $Tb_2Ti_2O_7$. *Phys. Rev. Lett.* **112,** 017203 (2014).
44. Madden, P. A., O'Sullivan, K. F. & Chiarotti, G. Ordering of the silver ions in α-AgI: a mechanism for the α-β phase transition. *Phys. Rev. B* **45,** 10206–10212 (1992).
45. Tucker, M. T., Squires, M. P., Dove, M. T. & Keen, D. A. Dynamic structural disorder in cristobalite: neutron total scattering measurement and reverse Monte Carlo modelling. *J. Phys. Condens. Matter* **13,** 403–423 (2001).
46. Levin, I., Krayzman, V. & Woicik, J. C. Local structure in perovskite (Ba,Sr)TiO_3: Reverse Monte Carlo refinements from multiple measurement techniques. *Phys. Rev. B* **89,** 024106 (2014).
47. Comès, R., Lambert, M. & Guinier, A. Désordre linéaire dans les cristaux (cas du silicium, du quartz, et des pérovskites ferroélectriques). *Acta Crystallogr. A* **26,** 244–254 (1970).
48. Božin, E. S. *et al.* Entropically stabilized local dipole formation in lead chalcogenides. *Science* **330,** 1660–1663 (2010).
49. Hull, S. *et al.* Neutron total scattering study of the delta and beta phases of Bi_2O_3. *Dalton Trans.* **2009,** 8737–8745 (2009).
50. Keeble, D. S. *et al.* Bifurcated polarization rotation in bismuth-based piezoelectrics. *Adv. Funct. Mater.* **23,** 185–190 (2013).
'Big-box' modelling of total scattering shows how the local polarization changes within a higher-symmetry average lattice.
51. Zhang, W., Cai, Y., Xiong, R.-G., Yoshikawa, H. & Awaga, K. Exceptional dielectric phase transitions in a perovskite-type cage compound. *Angew. Chem. Int. Ed.* **49,** 6608–6610 (2010).
52. Berret, J.-F., Bostoen, C. & Hennion, B. Phase diagram of the dipolar glass $K_{1-x}(NH_4)_xI$. *Phys. Rev. B* **46,** 13747–13750 (1992).
53. David, W. I. F., Ibberson, R. M., Dennis, T. J. S., Hare, J. P. & Prassides, K. Structural phase transitions in the fullerene C_{60}. *Europhys. Lett.* **18,** 219–225 (1992).
54. Liu, X. *et al.* Structural changes in a marine podovirus associated with release of its genome into *Prochlorococcus*. *Nature Struct. Mol. Biol.* **17,** 830–836 (2010).
55. Xu, G., Wen, J., Stock, C. & Gehring, P. M. Phase instability induced by polar nanoregions in a relaxor ferroelectric system. *Nature Mater.* **7,** 562–566 (2008).
56. Billinge, S. J. L., Proffen, Th., Petkov, V., Sarrao, J. L. & Kycia, S. Evidence for charge localization in the ferromagnetic phase of $La_{1-x}Ca_xMnO_3$ from high real-space-resolution x-ray diffraction. *Phys. Rev. B* **62,** 1203–1211 (2000).
57. Bennemann, K. H. & Ketterson, J. B. (eds) *Superconductivity: Conventional and Unconventional Superconductors* Vol. 1 (Springer, 2008).
58. Mühlbauer, S. *et al.* Skyrmion lattice in a chiral magnet. *Science* **323,** 915–919 (2009).
59. Bramwell, S. T. *et al.* Measurement of the charge and current of magnetic monopoles in spin ice. *Nature* **461,** 956–959 (2009).
60. Christensen, M. *et al.* Avoided crossing of rattler modes in thermoelectric materials. *Nature Mater.* **7,** 811–815 (2008).
61. Bowron, D. T. *et al.* NIMROD: The Near and InterMediate Range Order Diffractometer of the ISIS second target station. *Rev. Sci. Instrum.* **81,** 033905 (2010).
62. Cliffe, M. J. *et al.* Correlated defect nanoregions in a metal–organic framework. *Nature Commun.* **5,** 4176 (2014).
63. Rademacher, N., Daemen, L. L., Chronister, E. L. & Proffen, T. Pair distribution function analysis of molecular compounds: significance and modeling approach discussed using the example of *p*-terphenyl. *J. Appl. Cryst.* **45,** 482–488 (2012).
64. Goossens, D. J. & Whitfield, R. E. Distinguishing types of disorder in diffuse scattering: a numerical simulation study. *Metall. Mater. Trans. A* **45,** 152–161 (2014).
65. Krayzman, V. & Levin, I. Reverse Monte Carlo refinements of nanoscale atomic correlations using powder and single-crystal diffraction data. *J. Appl. Cryst.* **45,** 106–112 (2012).
66. Weber, T. & Simonov, A. The three-dimensional pair distribution function analysis of disordered single crystals: basic concepts. *Z. Kristallogr.* **227,** 238–247 (2012).
67. Danilkin, S. A. Diffuse scattering and lattice dynamics of superionic copper chalcogenides. *Solid State Ionics* **180,** 483–487 (2009).
68. Chang, L.-J. *et al.* Higgs transition from a magnetic Coulomb liquid to a ferromagnet in $Yb_2Ti_2O_7$. *Nature Commun.* **3,** 992 (2012).
69. Wehinger, B. *et al.* Diffuse scattering in Ih ice. *J. Phys. Condens. Matter* **26,** 265401 (2014).
High-quality X-ray diffuse and inelastic scattering and computer simulations are combined to show how the molecules in water ice disorder.
70. Kwei, G. H., Lawson, A. C., Billinge, S. J. L. & Cheong, S.-W. Structures of the ferroelectric phases of barium titanate. *J. Phys. Chem.* **97,** 2368–2377 (1993).
71. Algara-Siller, G. *et al.* Square ice in graphene nanocapillaries. *Nature* **519,** 443–445 (2015).
72. Bernal, J. D. & Fowler, R. H. A theory of water and ionic solution, with particular reference to hydrogen and hydroxyl ions. *J. Chem. Phys.* **1,** 515–548 (1933).
73. Lieb, E. H. Residual entropy of square ice. *Phys. Rev.* **162,** 162–172 (1967).

Acknowledgements We are grateful for discussions with J. A. M. Paddison, M. J. Cliffe and A. B. Cairns. A.L.G. acknowledges financial support from the ERC (grant number 279705).

Author Contributions D.A.K. and A.L.G. contributed equally to this work.

Author Information Reprints and permissions information is available at www.nature.com/reprints. The authors declare no competing financial interests. Readers are welcome to comment on the online version of the paper. Correspondence and requests for materials should be addressed to D.A.K. (david.keen@stfc.ac.uk) or A.L.G. (andrew.goodwin@chem.ox.ac.uk).